# Overexpression of Rhodopsin or Its Mutants Leads to Energy Metabolism Dysfunction in 661w Cells

Yang Liu,[1,2] Xin Wang,[1,2] Ruowen Gong,[1,2] Gezhi Xu,[1,2] and Min Zhu[1,2]

[1]Shanghai Key Laboratory of Visual Impairment and Restoration, Eye & ENT Hospital, Fudan University, Shanghai, China
[2]NHC Key Laboratory of Myopia (Fudan University); Key Laboratory of Myopia, Chinese Academy of Medical Sciences, Shanghai, China

Correspondence: Gezhi Xu, Shanghai Key Laboratory of Visual Impairment and Restoration, Eye & ENT Hospital, Fudan University, 83 Fenyang Road, Shanghai 200031, China;
der_winter@163.com.
Min Zhu, Shanghai Key Laboratory of Visual Impairment and Restoration, Eye & ENT Hospital, Fudan University, 83 Fenyang Road, Shanghai 200031, China;
081101015@fudan.edu.cn.

YL and XW contributed equally to the work presented here and should therefore be regarded as equivalent authors.

**PURPOSE.** Retinitis pigmentosa (RP) is a heterogeneous group of inherited disorders characterized by photoreceptor degeneration. The rhodopsin gene (*RHO*) is the most frequent cause of autosomal dominant RP (ADRP), yet it remains unclear how *RHO* mutations cause heterogeneous phenotypes. Energy failure is a main cause of the secondary cone death during RP progression; however, its role in primary rod death induced by ADRP *RHO* mutants is unknown.

**METHODS.** Three *RHO* missense mutations were chosen from different clinical classes. Wild-type (WT) RHO and its mutants, P23H (class B1), R135L (class A), and G188R (class B2), were overexpressed in 661w cells, a mouse photoreceptor cell line, and their effects on oxidative phosphorylation (OXPHOS) and aerobic glycolysis were compared separately.

**RESULTS.** Here, we report that energy failure is an early event in the cell death caused by overexpression of WT RHO and its mutants. RHO overexpression leads to OXPHOS deficiency, which might be a result of mitochondrial loss. Nonetheless, only in WT RHO and P23H groups, energy stress triggers AMP-activated protein kinase activation and metabolic reprogramming to increase glycolysis. Metabolic reprogramming impairment in R135L and G188R groups might be the reason why energy failure and cell injury are much more severe in those groups.

**CONCLUSIONS.** Our results imply that overexpression of RHO missense mutants have distinct impacts on the two energy metabolic pathways, which might be related to their heterogeneous phenotypes.

Keywords: retinitis pigmentosa, *RHO* mutants, photoreceptor degeneration, energy metabolism dysfunction

Retinitis pigmentosa (RP) is a heterogeneous group of inherited disorders, characterized by photoreceptor (PR) degeneration and progressive visual loss. Mutations in multiple genes are associated with RP, and the rhodopsin gene (*RHO*) was the first identified RP gene.[1] To date, over 150 mutations in *RHO* have been reported, and the vast majority are the most frequent cause of autosomal dominant RP (ADRP).[2] ADRP *RHO* mutations consist of two major clinical classes[3]: Class A families have early-onset severe rod dysfunction, and class B families have a later onset and less severe phenotype with a slower progression. Some class B families (B1) have a mild phenotype with regional variability, and other families (B2) exhibit diffuse disease of moderate severity. The heterogeneous phenotypes are likely related to the biochemical and cellular defects associated with *RHO* mutations.[4]

Many *RHO* mutations have been studied in vitro or in vivo, and great progress has been achieved, indicating that *RHO* mutations have distinct effects on the structure and function of the protein.[5,6] Over the years, several attempts have been made to classify *RHO* mutations based on their biochemical and cellular behaviors.[6–8] The latest one, by Athanasiou et al.,[6] has expanded the classification into seven categories, including misfolding and disruption of proteostasis, mislocalization and disrupted intracellular traffic, instability and altered function. Still, the classification scheme does not always correlate well with clinical severity. Moreover, quite a few *RHO* mutations could not be classified into any of the seven categories. Hence, there must be some unknown categories, and further investigation, especially from a novel perspective, is needed for better understanding the pathogenesis of *RHO* ADRP.

PRs are among the most energy-consuming and metabolically active cells in the body. Although PRs are neuronal cells, their energy metabolism is similar to that in cancer cells. Over 80% of glucose is used for aerobic glycolysis even when oxygen is sufficient.[9] Aerobic glycolysis not only provides biosynthetic intermediates for the constant renewal of the PR outer segment but is also responsible for around half of the adenosine triphosphate (ATP) production in PRs.[10] Energy metabolism in PRs reprograms between aerobic glycolysis and oxidative phosphorylation (OXPHOS)

under stress, which gives PRs a survival advantage over inner retinal neurons whose only energy source is OXPHOS.[11,12]

It has been suggested that energy failure plays a pivotal role in RP progression, as the secondary cone death could be the result of intracellular energy depletion.[11,13] Nevertheless, it is unclear whether energy metabolism dysfunction is also involved in primary rod death in RP. Here, we explored how ADRP *RHO* mutants affect energy metabolism in PRs. Wild-type (WT) RHO and its three missense mutants, P23H (class B1), R135L (class A), and G188R (class B2), were overexpressed in 661w cells, a mouse PR cell line, and their effects on OXPHOS and aerobic glycolysis were compared separately.

## MATERIALS AND METHODS

### Cell Culture and Chemicals

The 661w cells were grown in Dulbecco's Modified Eagle's Medium (DMEM) containing 10% fetal bovine serum. No retinal was added in the culture medium in the following experiments to avoid any contributions of RHO signaling. *N*-acetylcysteine (NAC, S1623) and 2-aminoethyl diphenylborinate (2-APB, S6657) were purchased from Selleck Chemicals (Houston, TX, USA), and Ru265 (SML2991) and Compound C (P5499) were obtained from Sigma-Aldrich (St. Louis, MO, USA).

### Plasmids and Transfection

Full-length human *RHO* complementary DNA (cDNA) was subcloned into pcDNA3.1 vector. P23H (68C>A), R135L (404G>T), and G188R (562G>A) mutants and cytoplasmic tail (c-tail, amino acids 310–348) truncation mutants (see Fig. 5A) were prepared with a KOD-Plus-Mutagenesis Kit (SMK-101; Toyobo, Osaka, Japan), and the entire cDNA sequence was checked for second-site errors. Cells were transfected using FuGENE HD Transfection Reagent (PRE2311; Promega, Madison, WI, USA).

### Flow Cytometry Analysis

As described before,[14] cell apoptosis and necrosis were analyzed by flow cytometry (Beckman Coulter, Brea, CA, USA) with an Annexin-VFITC/PI apoptosis detection kit (556547; BD Biosciences, San Jose, CA, USA). Cellular calcium levels, mitochondrial mass, mitochondrial reactive oxygen species (ROS), and calcium levels were detected by measuring the mean fluorescence intensity (MFI) with flow cytometry after loading cells with eBioscience Calcium Sensor Dye eFluor 514 (0.5 µM, 65-0859-70; Thermo Fisher Scientific, Waltham, MA, USA), MitoTracker Green FM (0.1 µM, M7514; Thermo Fisher Scientific), MitoSOX (0.5 µM, M36008; Thermo Fisher Scientific), and Rhod-2 AM cell permeant (0.5 µM, R1245MP; Thermo Fisher Scientific), respectively, for 30 minutes. A minimum of 10,000 cells were analyzed in each sample.

### Immunofluorescence Double-Staining

Cells were fixed in 4% paraformaldehyde for 30 minutes, permeabilized with 0.2% Triton X-100 for 30 minutes, and blocked with 10% fetal calf serum for 90 minutes. Cells were sequentially incubated with mouse monoclonal Anti-Rhodopsin primary antibody (ab98887; Abcam, Cambridge,

UK) overnight at 4°C and FITC-conjugated anti-mouse immunoglobulin G (IgG, 610-102-121; Rockland Immuno-chemicals, Pottstown, PA, USA) for 90 minutes at room temperature. Next, cells were incubated with rabbit primary antibodies against Calnexin (ab22595; Abcam) overnight at 4°C and Anti-Rabbit IgG (H&L) (Goat) Antibody Rhodamine Conjugated (611-1022; Rockland Immunochemicals) for 90 minutes. Cells were washed with PBS between stages, and images were taken by confocal laser-scanning microscopy (Leica Microsystems, Wetzlar, Germany).

### Bioenergetic Analyses

Cells were seeded into a luminometer plate the day before ATP measurement with a Luminescent ATP Detection Assay Kit (ab113849; Abcam). Luminescence was recorded with a Tecan luminescence reader (Tecan Group, Männedorf, Switzerland), and ATP concentrations in test samples were calculated from ATP standard curves and normalized to protein content measured using Pierce BCA Protein Assay Kit (23225; Thermo Fisher Scientific). The ADP/ATP ratio was detected with an ADP/ATP Ratio Assay Kit (Biolumi-nescent) (ab65313; Abcam). Reaction mix was added to a luminometer plate, and the background signal was read on the Tecan luminescence reader (Data A). Cells were treated with nucleotide releasing buffer and transferred to the lumi-nometer plate. Luminescence was recorded after reaction for 2 minutes (Data B) and read again before (Data C) and 2 minutes after adding ADP-converting enzyme (Data D): ADP/ATP ratio = (Data D – Data C)/(Data B – Data A). Each experiment was performed four times in three replicates.

### Seahorse Metabolism Analysis

Cells were seeded in an Agilent XF24 Cell Culture Plate (Agilent, Santa Clara, CA, USA) the day before analysis. The oxygen consumption rate (OCR) and the extracellular acidification rate (ECAR) were measured using an Agilent Seahorse XFe24 Analyzer. Cells were washed and incubated with Agilent Seahorse XF Base Medium (pH 7.4; 102353-100), supplemented with 2-mM L-glutamine, 10-mM glucose, and 1-mM sodium pyruvate, at 37°C without $CO_2$ for 1 hour before OCR measurements. After recording three baseline data, Oligomycin A (1 µM, 75351; Sigma-Aldrich), carbonyl cyanide-4-(trifluoromethoxy)phenylhydrazone (FCCP, 1 µM, C2920; Sigma-Aldrich), and rotenone (1 µM, R8875; Sigma-Aldrich) plus antimycin (1 µM, A8674; Sigma-Aldrich) were auto-injected into the wells, and three measurements were recorded following each injection.

Cells were washed and incubated with the Agilent Seahorse XF Glycolysis Stress Test Kit (pH 7.35) supplemented with 2-mM L-glutamine) at 37°C without $CO_2$ for 1 hour before ECAR measurements. After recording three baseline data, glucose (1 µM), oligomycin (1 µM), and 2-deoxyglucose (2-DG, 1 µM, D8375; Sigma-Aldrich) were auto-injected into the wells, and three measurements following each injection were recorded. Each measurement was normalized to the final cell number in the same well, and each experiment was carried out four times in three replicates. The following measurements were obtained:

- Basal respiration = (last measurement before Oligomycin injection) – (minimum measurement

after rotenone and antimycin A injection). This shows the respiration rate of the cell under baseline conditions.

- Maximal respiration = (maximum measurement after FCCP injection) – (minimum measurement after rotenone and antimycin A injection). This shows the maximum respiration rate that the cell can achieve.
- Spare respiratory capacity (SRC) = (maximal respiration) – (basal respiration). This shows the respiratory ability of the cell to meet an increased energy demand.
- Glycolysis = (maximum measurement before Oligomycin injection) – (last measurement before glucose injection). This shows the aerobic glycolysis rate of the cell under baseline conditions.
- Glycolytic capacity = (maximum measurement after Oligomycin injection) – (last measurement before glucose injection). This shows the maximum aerobic glycolysis rate that the cell can achieve.
- Glycolytic reserve = (glycolytic capacity) – (glycolysis). This shows the glycolytic ability of the cell to meet an increased energy demand.

### Measurements of the Activities of Mitochondrial Respiratory Chain Complex I to IV

Mitochondrial respiratory chain complex I to IV (CI-IV) was detected as described before.[15] Mitochondria were isolated, and the levels of CI-IV and citrate synthase (CS) activity were measured separately with a Mitochondrial Complex I Activity Colorimetric Assay Kit, a Succinate Dehydrogenase Activity Colorimetric Assay Kit, a Mitochondrial Complex III Activity Assay Kit, a Cytochrome Oxidase Activity Colorimetric Assay Kit, and a Citrate Synthase Activity Colorimetric Assay Kit (all from BioVision, Milpitas, CA, USA). Each experiment was performed in three replicates and repeated four times.

### Glucose Uptake Assay

Glucose uptake was detected with a Promega Glucose Uptake-Glo Assay Kit (J1342). To initiate glucose uptake, cells were washed with PBS and incubated with 50 µL of 2-DG (1 mM) in PBS for 10 minutes at room temperature. After the addition of 25 µL of Stop Buffer, 25 µL of Neutralization Buffer, and 100 µL of 2-DG–6-Phosphate Detection Reagent, cells were incubated for 1 hour at room temperature, and luminescence was recorded as relative light units with a Tecan luminescence reader and normalized to protein concentrations. Each experiment was carried out four times in three replicates.

### Measurement of the Activities of Rate-Limiting Glycolytic Enzymes

Cells were collected, lysed, and centrifuged. The activities of hexokinase (HK, K789-100; BioVision), phosphofructokinase (PFK, K776-100; BioVision), pyruvate kinase (PK, K709-100; BioVision), and lactate dehydrogenase (LDH, K726-500; BioVision) in the supernatants were measured using BioVision colorimetric activity assay kits. HK, PFK, and LDH activities are determined by enzymatic reactions, all eventually forming reduced nicotinamide adenine dinucleotide (NADH), a colorimetric (450 nm) product. PK activities are detected by a coupled enzyme assay, also resulting in a colorimetric (570 nm) product. The absorbance of samples was determined using a Tecan Spark microplate reader; 1 unit is the amount of enzyme in 1 µg of total protein that will generate 1.0 µmol of NADH/ pyruvate per minute at room temperature. Each experiment was performed four times in three replicates.

### Cytosolic and Plasma Membrane Protein Extraction

Cellular cytosolic and plasma membrane proteins were extracted using an Abcam Plasma Membrane Protein Extraction Kit (ab65400). Cells were harvested, homogenized, and centrifuged at 700$g$ for 10 minutes. The supernatants were centrifuged at 10,000$g$ for 30 minutes, and the resulting supernatants were used as the cytosolic fraction; the pellets were resuspended in the upper-phase solution and mixed with the lower-phase solution. After centrifugation at 1000$g$ for 5 minutes, the upper phase was collected, and the lower phase was mixed with the upper-phase solution and centrifuged again. The two upper phases were mixed with the lower-phase solution and centrifuged. The upper phase was diluted with water and centrifuged at top speed for 10 minutes, and the resulting pellets were purified plasma membrane proteins.

### Immunoblotting Analyses

Protein samples (10–20 µg) were run on 8% to 12% SDS-PAGE gels. Antibodies obtained from Abcam included mouse anti-RHO primary antibody (N-terminal, 1:1000) and Anti-beta Actin antibody (1:1000, ab8226); Anti-PFKFB2 antibody (ab234865); and rabbit primary antibodies against GRP78 (ab21685) and Recombinant Anti-Glucose Transporter GLUT1 antibody (1:1000, ab115730). Antibodies (all 1:1000) obtained from Cell Signaling Technology (Danvers, MA, USA) included Na+/K+ ATPase (3010), cytochrome $c$ (4272), $c$-cas3 (9661), Tom20 (42406), HKII (2867), phosphorylated PKM2 (p-PKM2, 3827), PKM2 (4053), LDHA (2012), AMP-activated protein kinase $\alpha$ (AMPK$\alpha$, 2532), and p-AMPK$\alpha$ (T172, 2535). Antibodies (all 1:2000) obtained from United Chemi-Con (Rolling Meadows, IL, USA) included horseradish peroxidase-conjugated secondary anti-rabbit IgG (AP132P) and anti-mouse IgG (AP308P).

### Statistical Analysis

The data are exhibited as mean $\pm$ SEM and were subjected to statistical analysis via one-way or two-way ANOVA. The level of statistical significance was set at $P < 0.05$.

## RESULTS

### Energy Failure and Cell Injury Were Much More Severe in the R135L and G188R Groups

The 661w cells were overexpressed with WT RHO. The protein levels of RHO in cells were detected by immunoblotting at 24, 36, 48, and 60 hours after transfection, and a plateau was reached at 48 hours (Fig. 1A). RHO levels were also measured at 48 hours after transfection with WT RHO and its missense mutants (P23H, R135L, and G188R), and they were robustly increased in each overexpressed group (Fig. 1A).
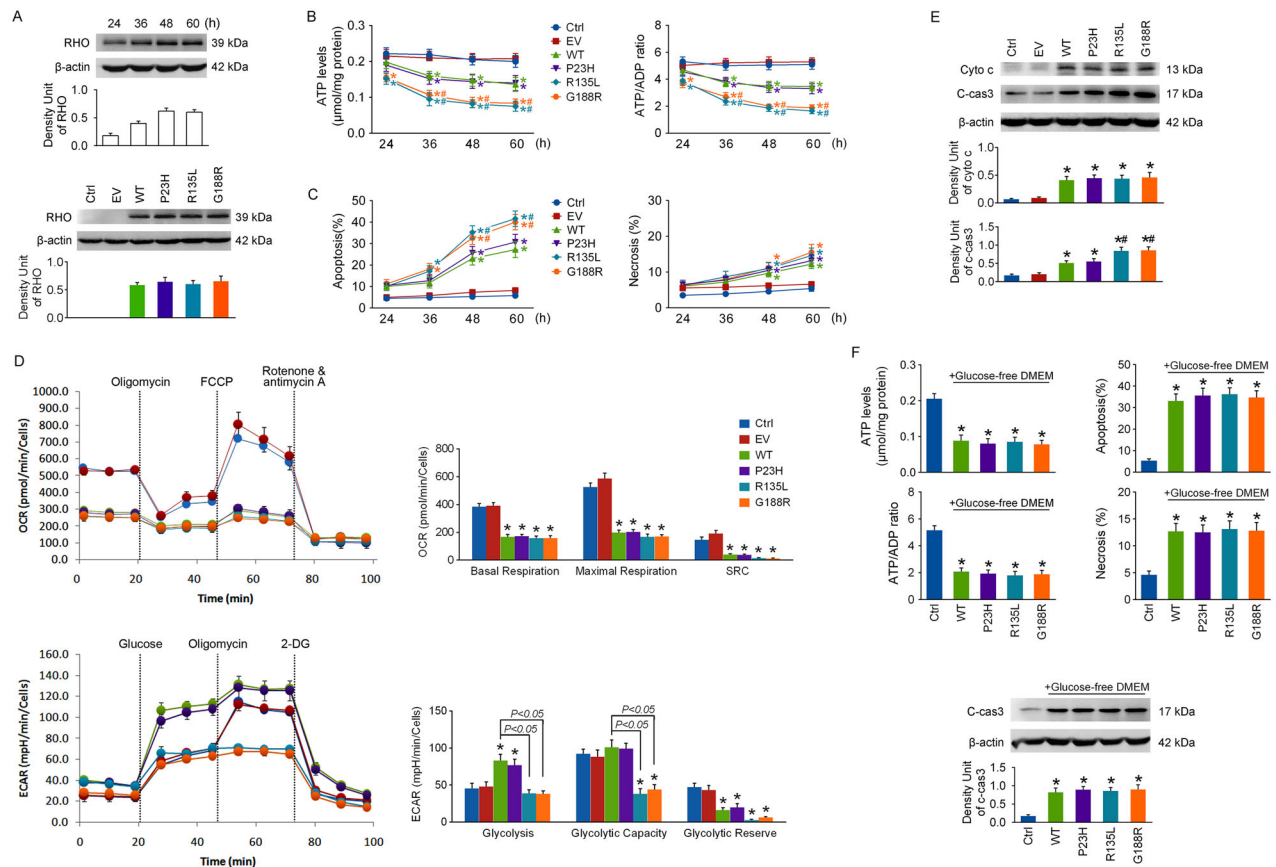
**FIGURE 1.** The effects of wild-type rhodopsin and its mutants on cell survival and energy production. (A) The 661w cells were overexpressed with WT RHO, and the protein levels of RHO in cells were detected by immunoblotting at 24, 36, 48, and 60 hours after transfection. Next, cells were overexpressed with WT RHO and its missense mutants (P23H, R135L, and G188R), and RHO levels were detected by immunoblotting at 48 hours after transfection. (B) Cellular ATP levels and ATP/ADP ratios in each group were detected at 24, 36, 48, and 60 hours after transfection. (C) Cell apoptosis and necrosis were determined by flow cytometry with an Annexin-V FITC/PI Apoptosis Detection Kit at 24, 36, 48, and 60 hours after transfection. (D) The OCR and ECAR were analyzed using an Agilent Seahorse XFe24 Analyzer at 48 hours after transfection. (E) The protein levels of cyto $c$ in the cytosolic fraction and c-cas3 were detected by immunoblotting at 48 hours after transfection. (F) The culture medium was changed to glucose-free DMEM at 24 hours after transfection, and the cellular energy status and cell apoptosis were determined after another 24 hours. *$P < 0.05$ compared with control group at the same time point, #$P < 0.05$ compared with the WT group at the same time point ($n = 4$).

Cellular ATP levels, ATP/ADP ratio, cell apoptosis, and necrosis were determined at 24, 36, 48, and 60 hours after transfection to compare the impacts of RHO overexpression on cell death and energy status. As shown in Figures 1B and 1C, RHO overexpression mainly caused cell apoptosis in 661w cells, and decreases in cellular ATP levels and the ATP/ADP ratio were induced much earlier than cell death in each RHO overexpressed group. This suggests that energy failure may be one of the early cell death events in all RHO overexpressed groups and that energy failure and cell injury were much more severe in the R135L and G188R groups.

## Energy Metabolic Reprogramming Impairment Is Likely the Reason Why Energy Failure and Cell Injury Were More Severe in the R135L and G188R Groups

OXPHOS was analyzed by OCR measurements and aerobic glycolysis by ECAR measurements at 48 hours after transfection. As shown in Figure 1D, mitochondrial basal and maxi-

mal respiration were drastically reduced in each RHO over-expressed group. Glycolysis was substantially enhanced, and the glycolytic reserve was remarkably decreased in WT RHO and P23H groups, implying that a glycolytic reserve might be mobilized to enhance basal glycolysis in these two groups as a response to decreased basal respiration. However, glycolysis was barely affected in R135L and G188R groups. The data suggest that OXPHOS deficiency was induced in each RHO overexpressed group, which triggered energy metabolic reprogramming to increase glycolysis only in the WT RHO and P23H groups.

Mitochondrial dysfunction plays a critical role in initiating cell apoptosis. The protein levels of cytochrome $c$ (cyto $c$) in the cytosolic fraction and cleaved caspase-3 (c-cas3), the final executor of apoptosis, were detected by immunoblotting at 48 hours after transfection. Mitochondrial cyto $c$ release was robustly elevated in each RHO overexpressed group. The c-cas3 levels were remarkably increased in WT RHO and P23H groups, and much higher in R135L and G188R groups (Fig. 1E). These data confirm that cell apoptosis was more severe in the R135L and G188R groups;
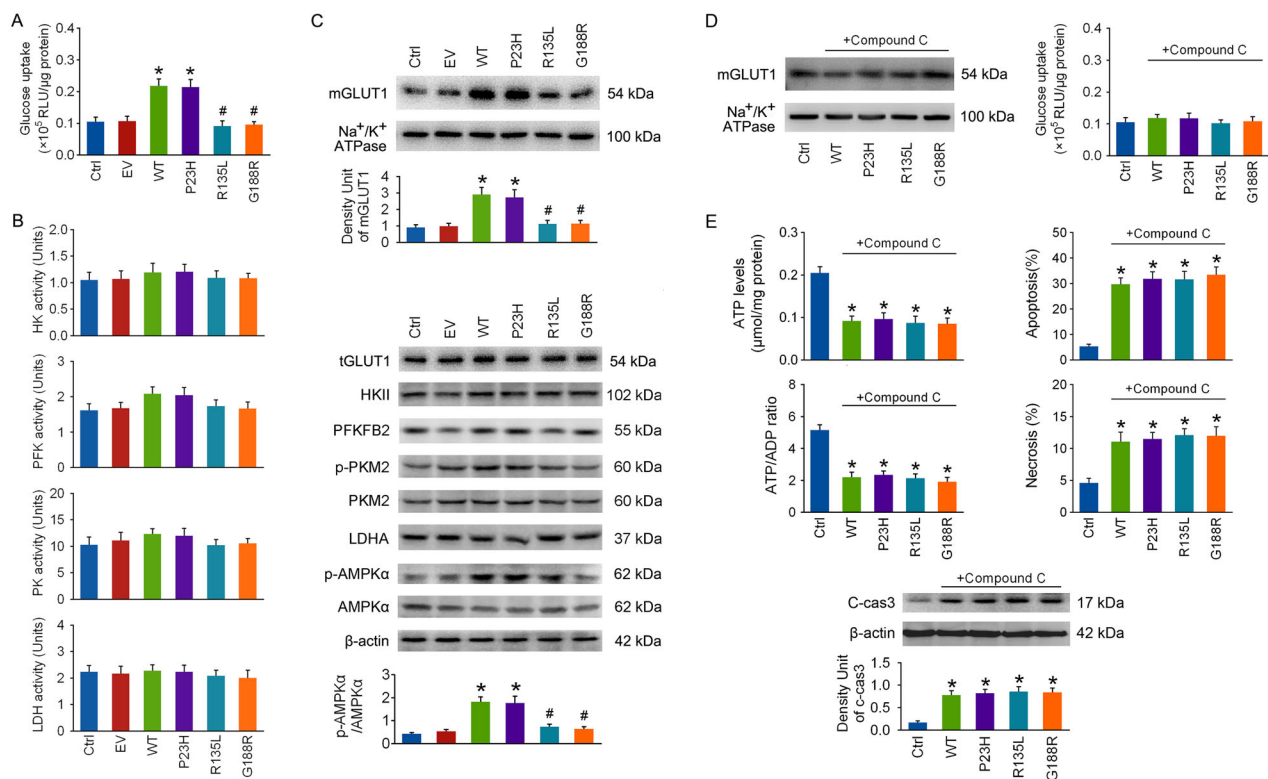
**FIGURE 2.** The influence of RHO overexpression on the rate-limiting steps of glycolysis. The 661w cells were transfected with WT RHO and its mutants. (A) Glucose uptake was measured with a glucose uptake assay kit at 48 hours after transfection. (B) The activities of HK, PFK, PK, and LDH in cells were measured using colorimetric activity assay kits at 48 hours after transfection. (C) The levels of GLUT1 in the plasma membrane fraction (mGLUT1), the total levels of GLUT1 in cells (tGLUT1), and the protein levels of HKII, PFKFB2, p-PKM2, PKM2, LDHA, p-AMPKα (T172), and AMPKα were detected by immunoblotting at 48 hours after transfection. (D) Compound C (1 μM) was applied to cells after transfection, and mGLUT1 levels and glucose uptake were determined at 48 hours. (E) Cellular energy status and cell apoptosis were assayed. *$P < 0.05$ compared with the control group, #$P < 0.05$ compared with the WT group ($n = 4$).

however, other mechanisms might be involved besides mitochondrial dysfunction.

To test the role of increased glycolysis in ATP production and cell death in WT RHO and P23H groups, the culture medium was changed to glucose-free DMEM at 24 hours after transfection to suppress glycolysis. As seen in Figure 1F, energy failure and cell apoptosis in WT RHO and P23H groups were worsened by glucose deprivation for 24 hours, suggesting that metabolic reprogramming impairment might be the reason why energy failure and cell injury were more severe in the R135L and G188R groups.

## Energy Stress Failed to Stimulate AMPK-Mediated Glucose Uptake in the R135L and G188R Groups

The first rate-limiting step of glycolysis is glucose uptake, which was detected with a glucose uptake assay kit at 48 hours after transfection; the other rate-limiting steps were monitored by measuring the activities of four key enzymes (HK, PFK, PK, and LDH) using colorimetric activity assay kits.[16] Glucose uptake was significantly increased only in the WT RHO and P23H groups (Fig. 2A), but the activities of the four key enzymes were barely affected in any group (Fig. 2B). The protein levels of hexokinase 2, 6-phosphofructo-2-kinase/fructose-2,6-bisphosphatase (PFKFB), p-PKM2, PKM2, and lactate

dehydrogenase A (LDHA) were barely affected in RHO overexpressed cells at 48 hours after transfection (Fig. 2C). These observations suggest that the elevation in glycolysis in the WT RHO and P23H groups was mainly due to enhanced glucose uptake.

Glucose uptake by PRs is mostly dependent on glucose transporter protein type 1 (GLUT1),[17,18] and an elevation in GLUT1 expression or the translocation of cytosolic GLUT1 to the plasma membrane surface can lead to enhanced glucose uptake.[19,20] As shown in Figure 2C, the levels of GLUT1 in the plasma membrane fraction (mGLUT1) were robustly elevated in the WT and P23H groups, whereas the total levels of GLUT1 in cells (tGLUT1) were barely affected in any group at 48 hours after transfection.

AMPK is a crucial cellular energy sensor,[21] and phosphorylation at T172 of AMPKα is essential for its activation.[22] The p-AMPKα/AMPKα ratio was significantly increased only in the WT and P23H groups at 48 hours after transfection (Fig. 2C), indicating that AMPK might have been selectively activated in the WT RHO and P23H groups. Compound C (1 μM), a specific AMPK inhibitor,[23] was applied to cells right after transfection. As shown in Figure 2D, the elevations in mGLUT1 levels and glucose uptake in WT RHO and P23H groups at 48 hours after transfection were completely reversed by Compound C, suggesting that the energy metabolic reprogramming in the WT RHO and P23H groups was prevented by AMPK inhibition. Addi-
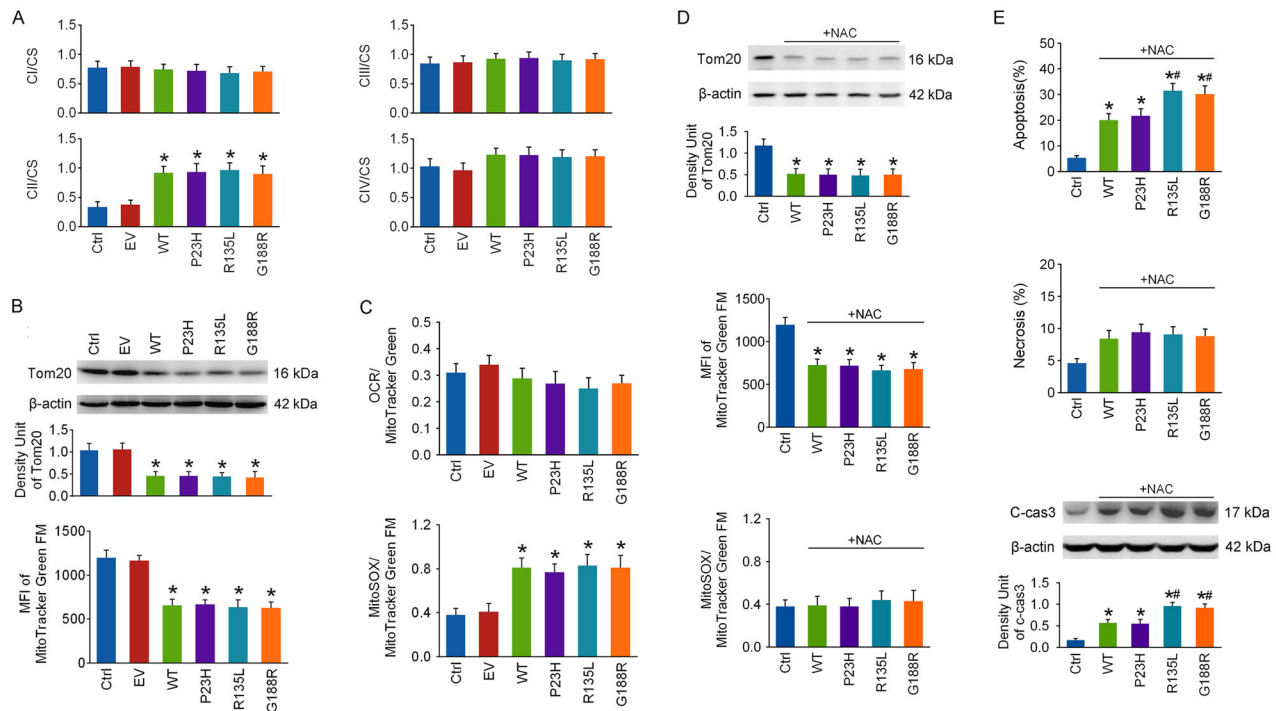
**FIGURE 3.** The impacts of WT RHO and its mutants on mitochondrial respiratory chain activities and mitochondrial mass. The 661w cells were transfected with WT RHO and its mutants. (A) Mitochondrial CI-CIV and CS activity were detected respectively at 48 hours after transfection, and the results of CI-CV (unit/mL) were normalized to CS (units/mL), a common marker enzyme for intact mitochondria. (B) The protein levels of Tom20, a protein marker of mitochondrial enrichment, were measured at 48 hours after transfection, and mitochondrial mass was also detected by measuring the MFI with flow cytometry after loading cells with MitoTracker Green FM. (C) To compensate for mitochondrial enrichment in cells, the OCR data for mitochondrial basal respiration were normalized to the MFI of MitoTracker Green FM in the same group. Mitochondrial ROS levels were detected by measuring the MFI of MitoSOX with flow cytometry at 48 hours after transfection, which was normalized to that of MitoTracker Green FM in the same group. (D) NAC (1 mM), a reactive oxygen species scavenger, was applied to cells after transfection. At 48 hours, mitochondrial mass was detected by measuring Tom20 levels and the MFI of MitoTracker Green FM, and mitochondrial ROS levels were assayed as described above. (E) Cellular energy status and cell apoptosis were tested. *$P < 0.05$ compared with the control group, #$P < 0.05$ compared with the WT group ($n = 4$).

tionally, energy failure and cell apoptosis in the WT and P23H groups were worsened by Compound C treatment (Fig. 2E).

## OXPHOS Deficiency in RHO Overexpressed Cells Is Likely Due to Massive Mitochondrial Loss

OXPHOS deficiency could be caused by the inhibition of mitochondrial respiratory chain activities or mitochondrial loss. Mitochondrial respiratory chain activities were determined at 48 hours after transfection. The CI/CS, CIII/CS, and CIV/CS ratios were barely affected, and the CII/CS ratio was even remarkably elevated in each RHO overexpressed group (Fig. 3A), indicating that the activities of the mitochondrial respiratory chain might not be suppressed in RHO overexpressed cells. Next, the levels of Tom20, a widely used protein marker of mitochondrial enrichment, were detected by immunoblotting at 48 hours after transfection, and they were dramatically reduced in each RHO overexpressed group (Fig. 3B). Mitochondrial mass was also determined by measuring the MFI of MitoTracker Green FM, a ΔΨm-independent mitochondrial dye,[24] with flow cytometry, and it was significantly decreased in each RHO overexpressed group (Fig. 3B). These data suggest that RHO overexpression leads to massive loss in mitochondrial

mass. To compensate for mitochondrial loss, basal respiration data from OCR measurements were normalized to the MFI of MitoTracker Green FM in the same group, and the ratio was barely affected in each RHO overexpressed group (Fig. 3C). This indicates that the decrease in basal respiration in RHO overexpressed cells may be a result of mitochondrial loss.

As seen in Figure 3C, the MitoSOX/MitoTracker Green FM ratio was remarkably increased in each RHO overexpressed group at 48 hours after transfection, suggesting that RHO overexpression leads to mitochondrial ROS overproduction. NAC (1 mM), a ROS scavenger,[25] was applied to cells right after transfection. Although NAC successfully prevented mitochondrial ROS overproduction in RHO overexpressed cells, it could not rescue mitochondrial loss at 48 hours (Fig. 3D). Cell apoptosis was hardly affected, but necrosis was alleviated by NAC in the RHO overexpressed groups (Fig. 3E).

## Mitochondrial Loss in RHO Overexpressed Cells Is Associated With Excessive Intracellular Calcium Release

As shown in Figure 4A, the Rhod-2 AM/MitoTracker Green FM ratio was robustly increased in each RHO overexpressed group at 48 hours after transfection, indicating that
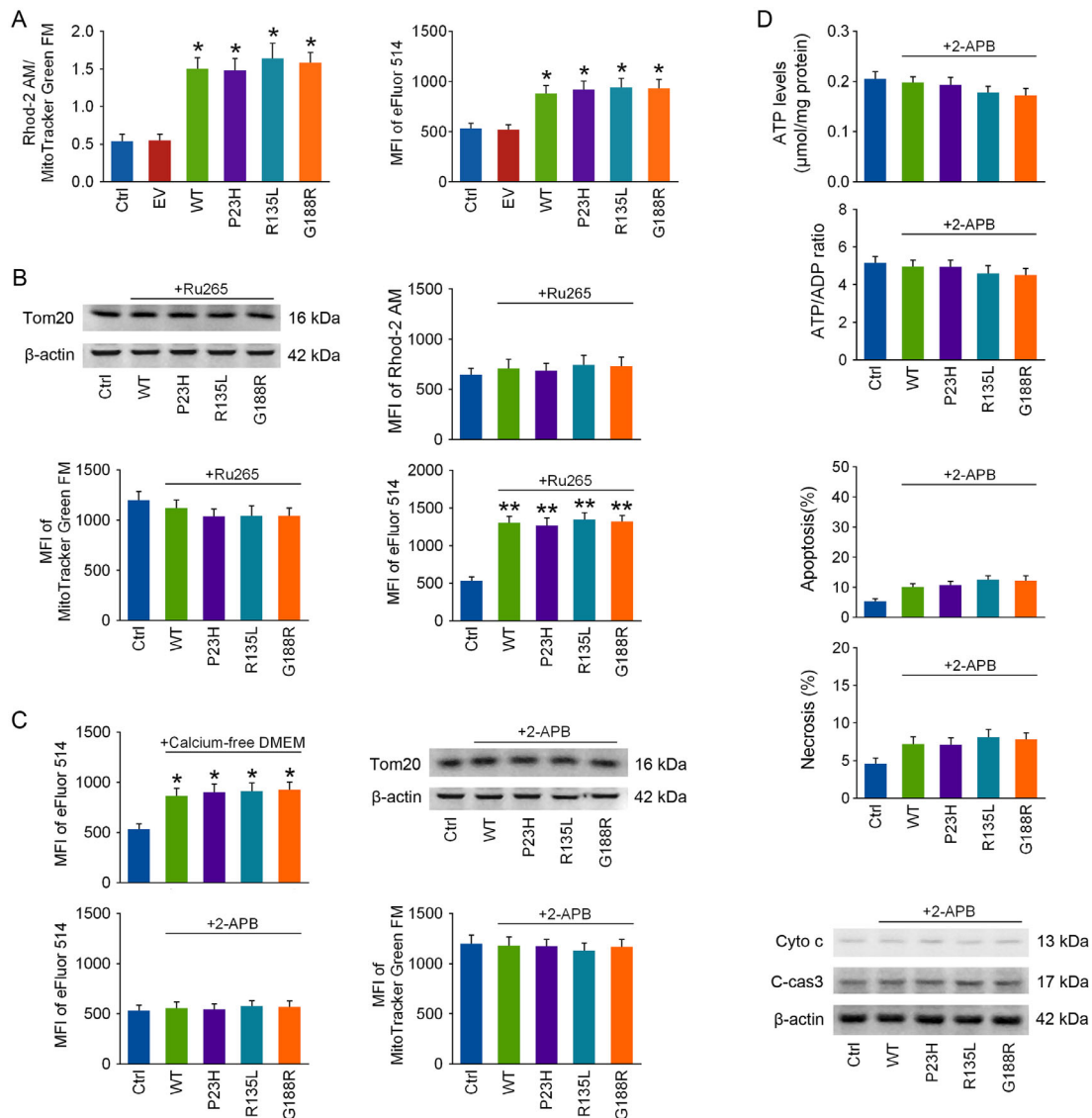
**FIGURE 4.** Inhibiting intracellular calcium release prevents the loss in mitochondrial mass in RHO overexpressed cells. The 661w cells were transfected with WT RHO and its mutants. (A) Mitochondrial and cellular calcium levels were determined by measuring the MFI of Rhod-2 AM and eFluor 514 with flow cytometry at 48 hours after transfection, and the MFI of Rhod-2 AM was further normalized to that of MitoTracker Green FM in the same group. (B) Ru265 (10 µM), a selective mitochondrial calcium uniporter inhibitor, was applied to cells after transfection, and mitochondrial mass and mitochondrial and cellular calcium levels were detected at 48 hours. (C) After transfection, either the culture medium was changed to calcium-free DMEM to prevent calcium influx or 2-APB (10 µM) was applied to cells to inhibit intracellular calcium release, and cellular calcium levels were detected at 48 hours. Mitochondrial mass was also assayed after 48 hours of 2-APB treatment. (D) Cellular energy status, cell apoptosis, and cyto *c* release from mitochondria were tested at 48 hours of 2-APB treatment. $*P < 0.05$, $**P < 0.01$ compared with the control group ($n = 4$).

RHO overexpression induces mitochondrial calcium overload. Mitochondrial calcium overload commonly results from cytosolic calcium overload, and the MFI of eFluor 514 was drastically increased in all the RHO overexpressed groups (Fig. 4A). Ru265 (10 µM), a selective mitochondrial calcium uniporter inhibitor,[26] was applied to cells right after transfection. Mitochondrial calcium overload was reversed, and the cytosolic calcium levels were even higher in RHO overexpressed cells after Ru265 treatment for 48 hours (Fig. 4B). More importantly, mitochondrial loss in each RHO overexpressed group was reversed by Ru265 treatment (Fig. 4B).

To determine whether cytosolic calcium overload in RHO overexpressed cells is a result of extracellular calcium influx or intracellular calcium release, the culture medium was changed into calcium-free DMEM after transfection to avoid calcium influx; however, it could not prevent cytosolic calcium overload in RHO overexpressed cells at 48 hours (Fig. 4C). Next, 2-APB (10 µM), an intracellular calcium release blocker,[27] was administrated to cells after transfection, and it completely prevented cytosolic calcium overload in RHO overexpressed cells at 48 hours (Fig. 4C). Moreover, mitochondrial loss (Fig. 4C), cyto *c* release, energy failure,
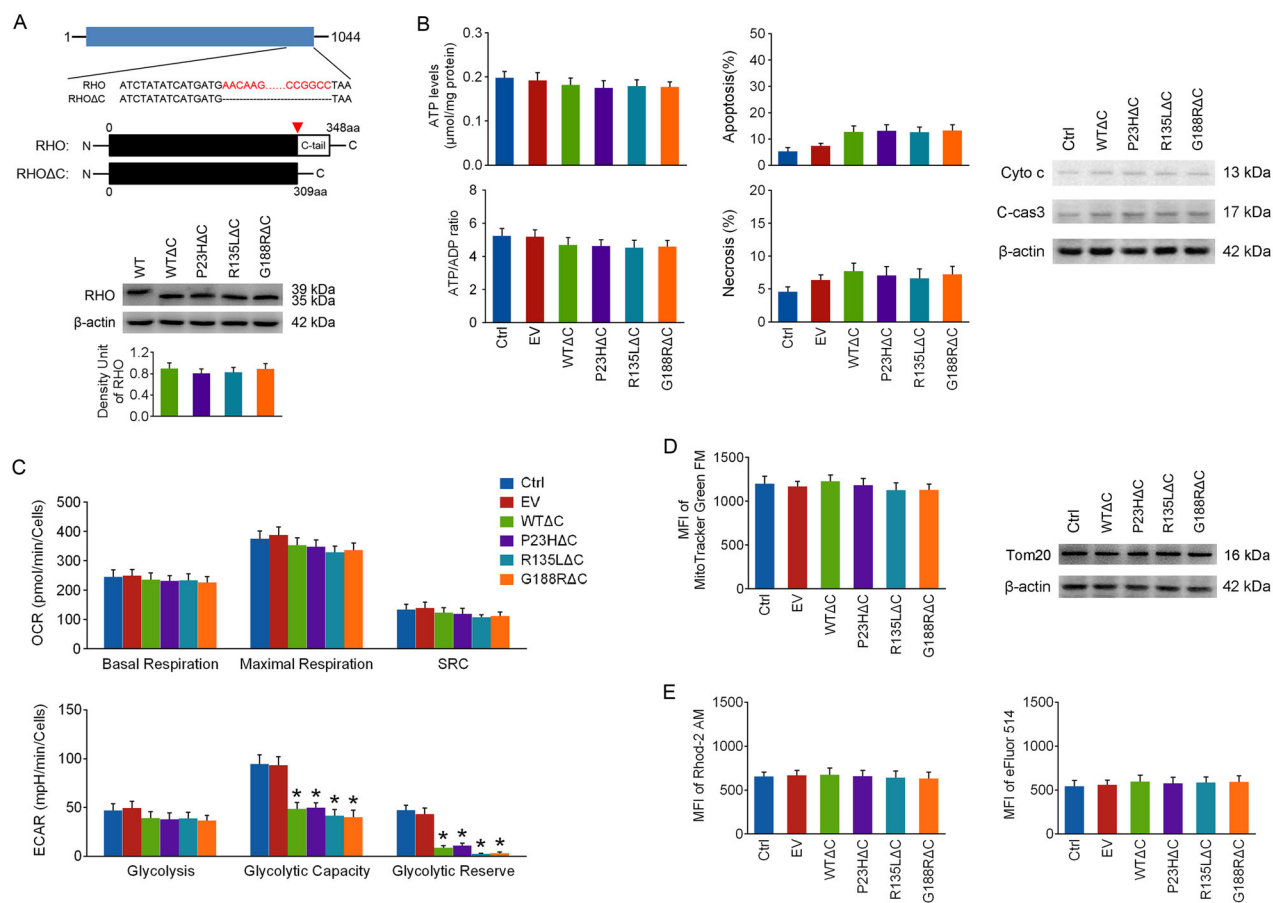
**FIGURE 5.** The effects of c-tail truncation on the toxicity of rho overexpression. (A) Diagram showing the structure of human RHO cDNA subcloned in the expression plasmid and the sequences of full-length RHO and its c-tail truncated mutant (RHOΔC). Their protein structures are shown below, and the *red arrowhead* marks the truncated site in RHOΔC (aa, amino acids). (B) The 661w cells were transfected with RHOΔC, and cellular energy status, cell apoptosis, and cyto *c* release from mitochondria were tested at 48 hours. (C) OCR and ECAR were detected as described above at 48 hours of transfection. (D) Mitochondrial mass was also assayed at 48 hours of transfection. (E) Mitochondrial and cellular calcium levels were analyzed. *$P < 0.05$ compared with the control group ($n = 4$).

and cell apoptosis (Fig. 4D) in RHO overexpressed cells were all reversed after 2-APB exposure for 48 hours.

## C-Tail Truncation of RHO Prevented OXPHOS Deficiency But Not Metabolic Reprogramming Impairment in Overexpressed Cells

It has been reported that the RHO c-tail might be toxic to PRs.[28] To test the effect of c-tail truncation on the toxicity of WT RHO and its mutants, the plasmids were all mutated to encode truncated proteins lacking c-tails. The resulting bands of RHOΔC (WTΔC, P23HΔC, R135LΔC, and G188RΔC) were approximately 4 kDa lower than that for WT RHO, and there was no appreciable statistical difference in RHO protein levels among the RHOΔC groups (Fig. 5A). As shown in Figures 5B and 5C, RHOΔC overexpression had little effect on energy status, cell death, cyto *c* release, or OXPHOS at 48 hours after transfection, yet the glycolytic capacity and glycolytic reserve were remarkably reduced in all of the RHOΔC overexpressed groups. These findings suggest that c-tail truncation might alleviate the toxicity of RHO overexpression by restoring OXPHOS. As seen

from Figures 5D and 5E, mitochondrial mass and cytosolic and mitochondrial calcium levels were barely affected in RHOΔC overexpressed cells, indicating that c-tail truncation of RHO may prevent mitochondrial loss and intracellular calcium release, as well.

## C-Tail Truncation Interrupted RHO Transport But Still Attenuated ER Stress

C-tail is crucial for RHO intracellular trafficking.[29] The localization of RHO and RHOΔC was observed at 48 hours after transfection by immunofluorescence double-staining of RHO and calnexin, an endoplasmic reticulum (ER) marker. As shown in Figure 6, the three mutants of RHO were mainly accumulated in ER, and c-tail truncation had little influence on their localization. However, WT RHO was barely co-localized with calnexin, whereas WTΔC was mainly accumulated in ER, confirming that the c-tail is required for RHO transport.

The protein levels of glucose-regulated protein 78 (GRP78) and C/EBP homologous protein (CHOP), both ER stress markers, were determined at 48 hours after
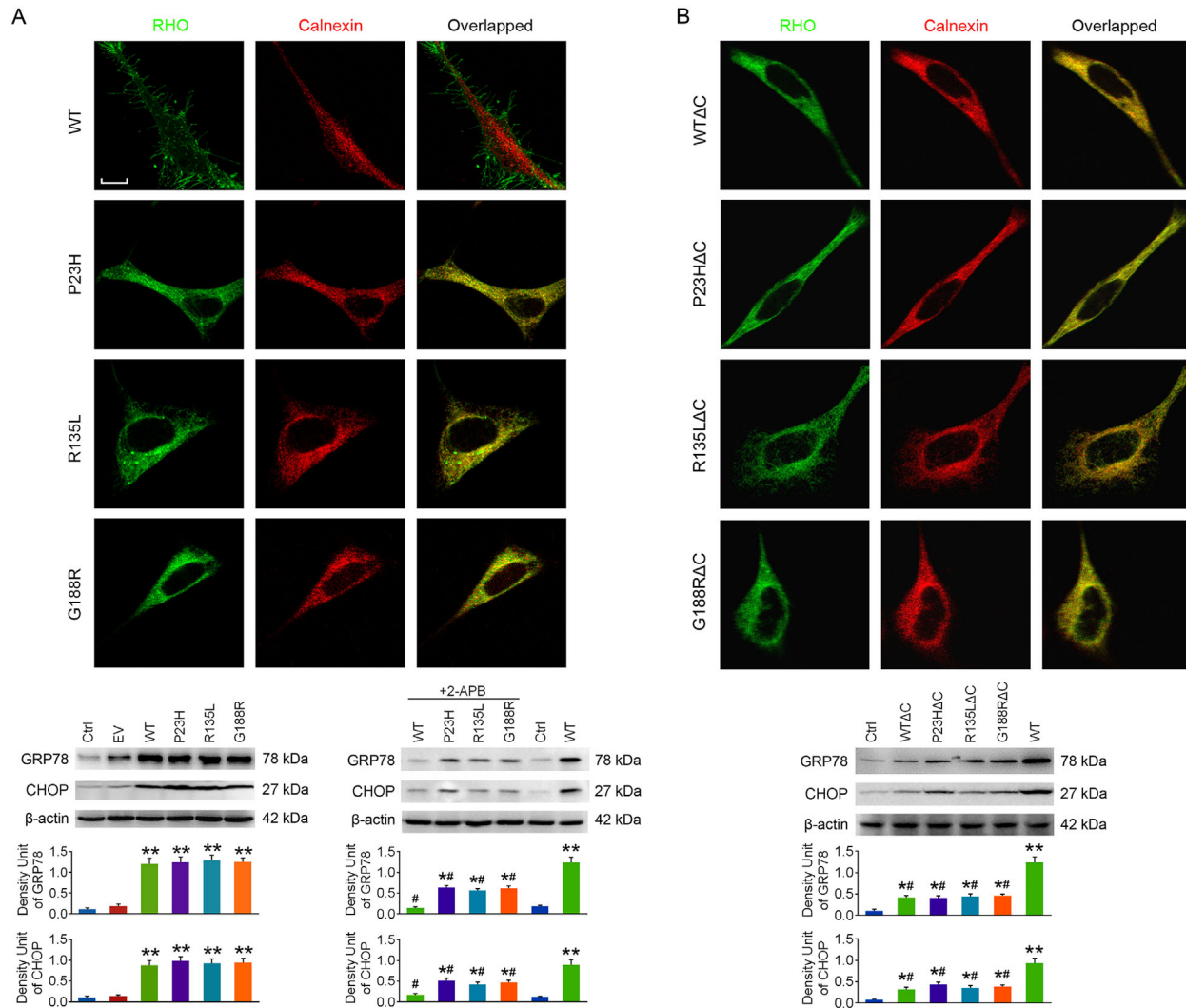
**FIGURE 6.** The effects of c-tail truncation on the localization of RHO and ER stress. The 661w cells were transfected with RHO or RHOΔC. (A) The localization of WT RHO, P23H, R135L, and G188R in cells was observed by immunofluorescence double-staining of RHO and calnexin at 48 hours after transfection. 2-APB was applied to cells after transfection, and the protein levels of GRP78 and CHOP, both ER stress markers, were detected at 48 hours. (B) The localization of WTΔC, P23HΔC, R135LΔC, and G188RΔC in cells was observed at 48 hours after transfection, and GRP78 and CHOP levels were also detected. *Scale bar*: 10 µm. *$P < 0.05$, **$P < 0.01$ compared with the control group; #$P < 0.05$ compared with the WT group with no drug treatment ($n = 4$).

transfection. To our surprise, GRP78 and CHOP levels were slightly elevated in each RHO overexpressed group (Fig. 6A) but only slightly increased in RHOΔC overexpressed cells (Fig. 6B). This observation suggests that the c-tail might contribute greatly to the severe ER stress in RHO overexpressed cells. Nevertheless, GRP78 and CHOP protein levels were slightly increased in the WTΔC group, suggesting that c-tail truncation of WT RHO might also lead to protein misfolding and mild ER stress.

Because it has been suggested that ER calcium depletion induces ER stress,[30] we next applied 2-APB to cells after transfection. We found that GRP78 and CHOP levels in RHO overexpressed cells were significantly reduced after 48 hours of 2-APB treatment (Fig. 6A), suggesting that ER stress in RHO overexpressed cells could be effectively alleviated by 2-APB.

## DISCUSSION

To the best of our knowledge, this is the first study to investigate the influences of overexpression of WT RHO and its missense mutants on energy metabolism in PRs. We found that energy failure is one of the early cell death events in RHO overexpressed cells, suggesting that, aside from being a cause of the secondary cone death in RP, it may be involved in primary rod death, as well. Therefore, energy metabolism dysfunction might play a key role in the pathogenesis of *RHO* ADRP. Because this present work was performed using cultured cells that could not entirely mimic PRs in vivo, our results still require confirmation by further investigation.

*RHO* mutants in our present study were chosen from various clinical classes. The data obtained demonstrate that cell injury was much more severe in the R135L and G188R groups than in the P23H group, which is generally correlated

with their clinical severity (R135L > G188R > P23H). This RHO overexpression cell model might be suitable to identify possible mechanisms underlying the heterogeneous phenotypes associated with *RHO* mutants. We further showed that energy failure was also more severe in the R135L and G188R groups, and impairment in metabolic reprogramming could be the reason why both energy failure and cell death were more severe in these two groups. Our observations confirm that metabolic reprogramming between OXPHOS and glycolysis is critical for PR survival under stress, and suggest that the distinct impacts of *RHO* mutants on the two energy metabolic pathways might be related to their heterogeneous phenotypes.

It has been suggested that, when activated by energy stress, AMPK promotes ATP production and restores cellular energy homeostasis,[21] including stimulating glucose uptake by enhancing GLUT1 expression,[31] surface translocation,[32] or activity.[33] As seen from our data reported here, AMPK activation in the WT RHO and P23H groups promotes glucose uptake by enhancing GLUT1 surface translocation, although it remains unknown whether GLUT1 activity is also affected. Meanwhile, energy stress failed to activate AMPK and initiate metabolic reprogramming to increase glycolysis in the R135L and G188R groups. The exact mechanism underlying this failure is not clear, and it might be some specific characteristics associated with the mutations that still require further investigation. It is noteworthy that the existing biochemical classifications of class II (misfolding; P23H, G188R) or class III (endocytosis; R135L) mutants do not directly correspond with the responses seen in this study, where R135L (class III) and G188R (class II) behaved similarly but P23H (class II) behaved differently.

Complexes I and II are the two entry points of the mitochondrial respiratory chain. However, because the Complex II pathway contributes less energy than the Complex I pathway, the Complex II pathway become the main source of SRC, and its activity only becomes manifest when energy demand increases or under energy stress.[34] We found that RHO overexpression in 661w cells caused an OXPHOS deficiency without suppressing mitochondrial respiratory chain activities. In fact, the CII/CS ratio was even significantly elevated, suggesting that SRC might be mobilized as a response to energy failure. This was further supported by the OCR data demonstrating that SRC in RHO overexpressed cells was reduced to almost zero.

Our investigation revealed that the c-tail might play a pivotal role of in the toxicity of WT RHO, as well as its mutants. C-tail truncation alleviated energy failure in each RHO overexpressed group by preventing OXPHOS deficiency but not metabolic reprogramming impairment. PRs have highly polarized structures, and the outer and inner segments are connected through a narrow channel referred to as the connecting cilium.[35] WT RHO is the main protein component of disc membranes in the outer segment, whereas organelles, such as the ER and mitochondria, are merely localized in the inner segment. This highly region-specific localization separates WT RHO from the ER and mitochondria, which might prevent the toxicity of WT RHO in normal PRs. It has long been recognized that overexpressed WT RHO could be toxic and trigger PR degeneration in vivo.[36] Therefore, another reason why WT RHO is toxic in 661w cells but not in normal PRs may be associated with the extreme high expression levels after overexpression. In addition, 11-*cis*-retinal binds to RHO in normal PRs and probably has some effect on its toxicity.

In conclusion, we have reported here that energy failure is one of the early cell death events after overexpression of WT RHO and its missense mutants in 661w cells. RHO overexpression led to OXPHOS deficiency, which triggered AMPK activation and metabolic reprogramming to increased aerobic glycolysis only in the WT RHO and P23H groups. Metabolic reprogramming impairment in the R135L and G188R groups might be the reason why energy failure and cell injury were much more severe in those groups. Our results suggest that overexpression of RHO missense mutants may have distinct impacts on energy metabolism that are possibly related to their heterogeneous phenotypes.

## References

1. Dryja TP, McGee TL, Reichel E, et al. A point mutation of the rhodopsin gene in one form of retinitis-pigmentosa. *Nature*. 1990;343(6256):364–366, https://doi.org/10.1038/343364a0.

2. Chapple JP, Grayson C, Hardcastle AJ, Saliba RS, van der Spuy J, Cheetham ME. Unfolding retinal dystrophies: a role for molecular chaperones? *Trends Mol Med*. 2001;7(9):414–421, https://doi.org/10.1016/S1471-4914(01)02103-7.

3. Cideciyan AV, Hood DC, Huang YJ, et al. Disease sequence from mutant rhodopsin allele to rod and cone photoreceptor degeneration in man. *Proc Natl Acad Sci USA*. 1998;95(12):7103–7108, https://doi.org/10.1073/pnas.95.12.7103.

4. Newton F, Megaw R. Mechanisms of photoreceptor death in retinitis pigmentosa. *Genes (Basel)*. 2020;11(10):1120, https://doi.org/10.3390/Genes11101120.

5. Sudharsan R, Beltran WA. Progress in gene therapy for rhodopsin autosomal dominant retinitis pigmentosa. *Adv Exp Med Biol*. 2019;1185:113–118.

6. Athanasiou D, Aguila M, Bellingham J, et al. The molecular and cellular basis of rhodopsin retinitis pigmentosa reveals potential strategies for therapy. *Prog Retin Eye Res*. 2018;62:1–23, https://doi.org/10.1016/j.preteyeres.2017.10.002.

7. Mendes HF, van der Spuy J, Chapple JP, Cheetham ME. Mechanisms of cell death in rhodopsin retinitis pigmentosa: implications for therapy. *Trends Mol Med*. 2005;11(4):177–185, https://doi.org/10.1016/j.molmed.2005.02.007.

8. Rakoczy EP, Kiel C, McKeone R, Stricher F, Serrano L. Analysis of disease-linked rhodopsin mutations based on structure, function, and protein stability calculations. *J Mol Biol*. 2011;405(2):584–606, https://doi.org/10.1016/j.jmb.2010.11.003.

9. Ng SK, Wood JPM, Chidlow G, et al. Cancer-like metabolism of the mammalian retina. *Clin Exp Ophthalmol*. 2015;43(4):367–376, https://doi.org/10.1111/ceo.12462.

10. Wang W, Kini A, Wang YK, et al. Metabolic deregulation of the blood-outer retinal barrier in retinitis pigmentosa.

*Cell Rep.* 2019;28(5):1323.e4, https://doi.org/10.1016/j.celrep.2019.06.093.

11. Petit L, Ma S, Cipi J, et al. Aerobic glycolysis is essential for normal rod function and controls secondary cone death in retinitis pigmentosa. *Cell Rep.* 2018;23(9):2629–2642, https://doi.org/10.1016/j.celrep.2018.04.111.

12. Wubben TJ, Pawar M, Smith A, Toolan K, Hager H, Besirli CG. Photoreceptor metabolic reprogramming provides survival advantage in acute stress while causing chronic degeneration. *Sci Rep.* 2017;7:17863, https://doi.org/10.1038/S41598-017-18098-Z.

13. Ait-Ali N, Fridlich R, Millet-Puel G, et al. Rod-derived cone viability factor promotes cone survival by stimulating aerobic glycolysis. *Cell.* 2015;161(4):817–832, https://doi.org/10.1016/j.cell.2015.03.023.

14. Liu Y, Zhu M, Gong RW, Wang X, Li L, Xu GZ. Pretreatment with ranibizumab aggravates PDT injury and alleviates inflammatory response in choroid-retinal endothelial cells. *Front Cell Dev Biol.* 2020;8:608, https://doi.org/10.3389/Fcell.2020.00608.

15. Ma HH, Liu Y, Tang L, et al. Echinacoside selectively rescues complex I inhibition-induced mitochondrial respiratory impairment via enhancing complex II activity. *Neurochem Int.* 2019;125:136–143, https://doi.org/10.1016/j.neuint.2019.02.012.

16. Li XB, Gu JD, Zhou QH. Review of aerobic glycolysis and its key enzymes - new targets for lung cancer therapy. *Thorac Cancer.* 2015;6(1):17–24, https://doi.org/10.1111/1759-7714.12148.

17. Gospe SM, Baker SA, Arshavsky VY. Facilitative glucose transporter Glut1 is actively excluded from rod outer segments. *J Cell Sci.* 2010;123(21):3639–3644, https://doi.org/10.1242/jcs.072389.

18. Mantych GJ, Hageman GS, Devaskar SU. Characterization of glucose-transporter isoforms in the adult and developing human eye. *Endocrinology.* 1993;133(2):600–607, https://doi.org/10.1210/En.133.2.600.

19. Al Mamun A, Hayashi H, Yamamura A, Nayeem MJ, Sato M. Hypoxia induces the translocation of glucose transporter 1 to the plasma membrane in vascular endothelial cells. *J Physiol Sci.* 2020;70(1):44, https://doi.org/10.1186/S12576-020-00773-Y.

20. Roy S, Leidal AM, Ye J, Ronen SM, Debnath J. Autophagy-dependent shuttling of TBC1D5 controls plasma membrane translocation of GLUT1 and glucose uptake. *Mol Cell.* 2017;67(1):84, https://doi.org/10.1016/j.molcel.2017.05.020.

21. Hardie DG, Ross FA, Hawley SA. AMPK: a nutrient and energy sensor that maintains energy homeostasis. *Nat Rev Mol Cell Biol.* 2012;13(4):251–262, https://doi.org/10.1038/nrm3311.

22. Oakhill JS, Steel R, Chen ZP, et al. AMPK is a direct adenylate charge-regulated protein kinase. *Science.* 2011;332(6036):1433–1435, https://doi.org/10.1126/science.1200094.

23. Liu XN, Chhipa RR, Nakano I, Dasgupta B. The AMPK inhibitor compound C is a potent AMPK-independent antiglioma agent. *Mol Cancer Ther.* 2014;13(3):596–605, https://doi.org/10.1158/1535-7163.MCT-13-0579.

24. Puleston D. Detection of mitochondrial mass, damage, and reactive oxygen species by flow cytometry. *Cold Spring Harb Protoc.* 2015;2015(9):pdb prot086298, https://doi.org/10.1101/pdb.prot086298.

25. Zhang FJ, Lau SS, Monks TJ. The cytoprotective effect of *N*-acetyl-L-cysteine against ROS-induced cytotoxicity is independent of its ability to enhance glutathione synthesis. *Toxicol Sci.* 2011;120(1):87–97, https://doi.org/10.1093/toxsci/kfq364.

26. Novorolsky RJ, Nichols M, Kim JS, et al. The cell-permeable mitochondrial calcium uniporter inhibitor Ru265 preserves cortical neuron respiration after lethal oxygen glucose deprivation and reduces hypoxic/ischemic brain injury. *J Cereb Blood Flow Metab.* 2020;40(6):1172–1181, https://doi.org/10.1177/0271678x20908523.

27. Hu WY, He ZY, Yang LJ, Zhang M, Xing D, Xiao ZC. The $Ca^{2+}$ channel inhibitor 2-APB reverses $\beta$-amyloid-induced LTP deficit in hippocampus by blocking BAX and caspase-3 hyperactivation. *Br J Pharmacol.* 2015;172(9):2273–2285, https://doi.org/10.1111/bph.13048.

28. Feng D, Chen Z, Yang K, et al. The cytoplasmic tail of rhodopsin triggers rapid rod degeneration in kinesin-2 mutants. *J Biol Chem.* 2017;292(42):17375–17386, https://doi.org/10.1074/jbc.M117.784017.

29. Tai AW, Chuang JZ, Bode C, Wolfrum U, Sung CH. Rhodopsin's carboxy-terminal cytoplasmic tail acts as a membrane receptor for cytoplasmic dynein by binding to the dynein light chain Tctex-1. *Cell.* 1999;97(7):877–887, https://doi.org/10.1016/s0092-8674(00)80800-4.

30. Mekahli D, Bultynck G, Parys JB, De Smedt H, Missiaen L. Endoplasmic-reticulum calcium depletion and disease. *Cold Spring Harb Perspect Biol.* 2011;3(6):a004317, https://doi.org/10.1101/cshperspect.a004317.

31. Sokolovska J, Isajevs S, Sugoka O, et al. Influence of metformin on GLUT1 gene and protein expression in rat streptozotocin diabetes mellitus model. *Arch Physiol Biochem.* 2010;116(3):137–145.

32. Lee CT, Ussher JR, Mohammad A, Lam A, Lopaschuk GD. 5′-AMP-activated protein kinase increases glucose uptake independent of GLUT4 translocation in cardiac myocytes. *Can J Physiol Pharmacol.* 2014;92(4):307–314, https://doi.org/10.1139/cjpp-2013-0107.

33. Barnes K, Ingram JC, Porras OH, et al. Activation of GLUT1 by metabolic and osmotic stress: potential involvement of AMP-activated protein kinase (AMPK). *J Cell Sci.* 2002;115(11):2433–2442, https://doi.org/10.1242/jcs.115.11.2433.

34. Vercellino I, Sazanov LA. The assembly, regulation and function of the mitochondrial respiratory chain. *Nat Rev Mol Cell Biol.* 2022;23(2):141–161, https://doi.org/10.1038/s41580-021-00415-0.

35. Kennedy B, Malicki J. What drives cell morphogenesis: a look inside the vertebrate photoreceptor. *Dev Dyn.* 2009;238(9):2115–2138, https://doi.org/10.1002/dvdy.22010.

36. Tan E, Wang Q, Quiambao AB, et al. The relationship between opsin overexpression and photoreceptor degeneration. *Invest Ophthalmol Vis Sci.* 2001;42(3):589–600.